

Some experimental schemes to identify quantum spin liquids

Yong Hao Gao¹ and Gang Chen^{2,1}

¹State Key Laboratory of Surface Physics and Department of Physics, Fudan University, Shanghai 200433, China and

²Department of Physics and HKU-UCAS Joint Institute for Theoretical and Computational Physics at Hong Kong, The University of Hong Kong, Hong Kong, China
(Dated: October 8, 2021)

Despite the apparent ubiquity and variety of quantum spin liquids in theory, experimental confirmation of spin liquids remains to be a huge challenge. Motivated by the recent surge of evidences for spin liquids in a series of candidate materials, we highlight the experimental schemes, involving the thermal transport and spectrum measurements, that can result in smoking-gun signatures of spin liquids beyond the usual ones. For clarity, we investigate the square lattice spin liquids and theoretically predict the possible phenomena that may emerge in the corresponding spin liquids candidates. The mechanisms for these signatures can be traced back to either the intrinsic characters of spin liquids or the external field-driven behaviors. Our conclusion does not depend on the geometry of lattices and can broadly apply to other relevant spin liquids.

I. INTRODUCTION

The search for exotic states in quantum magnets has been a central topic of intensive investigation in modern condensed matter physics. Among the various novel quantum states, quantum spin liquid (QSL), a non-symmetry-breaking phase beyond conventional Landau paradigm, is particularly appealing due to its potentially relevant to high-temperature superconductivity [1] and quantum-computation applications [2], in which the localized spins are highly entangled and remain disordered even down to zero temperature [3–5]. The concept of QSL was originally proposed by Anderson in 1973 when he studied the nearest neighbor antiferromagnetical Heisenberg model on triangular lattice [6]. Although the true ground state of this model has turned out to be a 120° magnetically ordered state, it does ignite the investigations of QSLs and the interplay between frustration and quantum fluctuation. Theoretically, various QSL ground states has been proposed, which are usually characterized by fractional spinons strongly coupled to emergent gauge field. In particular, Kitaev proposed [2] an exactly solvable spin-1/2 model on the honeycomb lattice in 2006, in which the presence of bond-dependent Kitaev interactions induces strong quantum fluctuations frustrating the spin configurations and resulting in a Kitaev QSL state.

From the experimental point of view, the kagomé, hyperkagomé and pyrochlore lattice materials with corner-sharing geometries or the edge-sharing triangular lattice materials provide ideal platforms to realize such an exotic magnetic ground state. In most QSL candidates, the results from measurements such as magnetization, heat capacity and nuclear magnetic resonance are consistent with properties of QSLs [3–5] and show no onset of long-range order at low temperatures. Besides, the crucial signature of a QSL is the presence of deconfined and fractionalized spinons that can be directly measured by inelastic neutron scattering and revealed in the excitation continuum, which is fundamentally different from the sharp and coherent magnon modes in ordered magnets. The magnetic excitation continuum indeed has been observed in geometrically frustrated spin-1/2 systems with both two-dimensional (2D) and three-dimensional (3D) lattices [7–10]. However, it has been shown that a simple spectral continuum may also originate from a spin glass state or disorder-

induced state [11–13]. Thus most experimental evidences so far are not strong enough to completely confirm a QSL.

Here we highlight the experimental schemes that would give smoking-gun signatures of QSLs beyond the usual ones mentioned above, including the thermal transport and spectrum measurements. First, we note that the π -flux QSL states would result in an enhanced spectral periodicity of the spinon continuum. It is the translation symmetry that is intrinsically fractionalized and renders such an enhanced spectral periodicity [14–16], much analogous to the fractional charge excitation in the fractional quantum Hall states where the global U(1) charge conservation gives the fractional charge quantum number to the fractionalized excitation [17]. Second, the Zeeman coupling will enter the spinon Hamiltonian under moderate magnetic fields, which can lead to an X-shaped crossing of spectrum compatible with the splitting spinon bands. The third case is a chiral spin liquid (CSL) that would exhibit a quantized thermal Hall effect and a gapped spectrum. In this work, we explicitly demonstrate these strong and non-trivial experimental signatures by considering square lattice QSLs, but we stress that our conclusion does not depend on the geometry of lattice and can generally apply to other relevant QSLs.

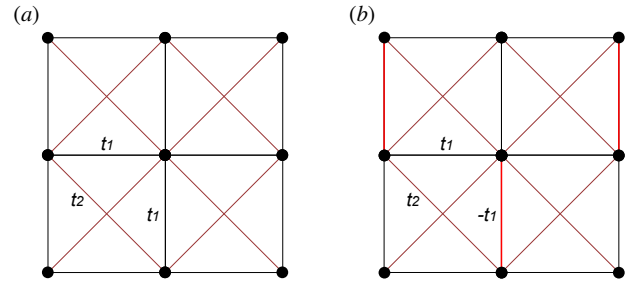


FIG. 1. Schematic illustration of spinon hoppings up to second neighbors on the square lattice. (a) The zero-flux QSL with a uniform nearest-neighbor spinon hopping coefficient $t_{1,ij} = t_{1,ji} = t_1$ and next-nearest-neighbor spinon hopping coefficient $t_{2,ij} = t_{2,ji} = t_2$. (b) The π -flux QSL with a gauge fixing such that the red thick lines stand for negative spinon hopping coefficient $t_{1,ij} = t_{1,ji} = -t_1$, while the meaning of other lines remains unchanged.

The remaining parts of the paper are structured as follows. In Sec. II, we introduce the Abrikosov fermion construction for the square lattice J_1 - J_2 Heisenberg model and illustrate the enhanced spectral periodicity for π flux QSL at the mean field level. In Sec. III, we explain the spectrum crossing under magnetic fields, which is well compatible with Zeeman-split spinon bands. In Sec. IV, we consider the ring-exchange term in the weak Mott insulating regime and show the integer quantized thermal Hall effect if the ground state is driven into a CSL phase. We conclude in Sec. V with a discussion of the results.

II. ENHANCED SPECTRAL PERIODICITY OF THE SPINON CONTINUUM

The discovery of fractional quantum Hall effect experimentally realized the theoretical concepts of emergence and fractionalization [18, 19]. The QSL is another obvious case of fractionalization [14], especially the π -flux QSL that owns fractionalized translation symmetry, and such a fractionalization would result in an observable phenomenon in experiment. For clarity, we begin with a J_1 - J_2 Heisenberg model on the 2D square lattice, which has attracted enormous research interests due to its intimate relation to the magnetism in high-temperature superconducting materials [1, 20], but we would not only constrain ourselves in this model. The Hamiltonian of J_1 - J_2 model is given by,

$$H = J_1 \sum_{\langle ij \rangle} \mathbf{S}_i \cdot \mathbf{S}_j + J_2 \sum_{\langle\langle ij \rangle\rangle} \mathbf{S}_i \cdot \mathbf{S}_j, \quad (1)$$

where \mathbf{S}_i is the spin-1/2 operator at the site i , $J_1 > 0$ and $J_2 > 0$ are the nearest-neighbor (NN) and next-nearest-neighbor (NNN) couplings. Moreover, the sums $\langle ij \rangle$ and $\langle\langle ij \rangle\rangle$ run over NN and NNN pairs, respectively. Although there is no geometrical frustration on a square lattice, by switching on an antiferromagnetic J_2 term indeed brings competing interactions and is expected, with the aid of quantum fluctuations, to destroy the conventional antiferromagnetic Néel state and result in a quantum disordered QSL. In fact, for the small J_2 region, just as the NN Heisenberg model on a square lattice, the ground state is generally believed to be a (π, π) long-ranged Néel order. On the other hand, when J_2 becomes comparable to J_1 , the $(\pi, 0)$ and $(0, \pi)$ stripe long-range order is stabilized [21–25]. For the intermediate region $0.4 \lesssim J_2/J_1 \lesssim 0.6$, it has been interpreted as the magnetically disordered QSL phase with either gapless or gapped excitations in various numerical studies [21–25]. We mainly focus on the intermediate disordered regime in this work and assume it realizes a QSL.

A. Abrikosov fermion construction

To analyze the QSL phase of this model, we here adopt the well-known and widely-used Abrikosov fermion construction since it can be utilized to study both gapped and gapless

phases, while the Schwinger boson formalism has the limitation to study gapped phases [26]. In the Abrikosov fermion representation, the effective spin-1/2 operator \mathbf{S}_i on site i is given by

$$\mathbf{S}_i = \frac{1}{2} \sum_{\alpha, \beta} f_{i\alpha}^\dagger \boldsymbol{\sigma}_{\alpha\beta} f_{i\beta} \quad (2)$$

where $f_{i,\alpha}^\dagger$ ($f_{i,\alpha}$) creates (annihilates) a spinon with the spin index $\alpha = \uparrow, \downarrow$ at site i , and $\boldsymbol{\sigma}$ is a vector of three Pauli matrices. The Hilbert space constraint $\sum_{\alpha} f_{i\alpha}^\dagger f_{i\alpha} = 1$ on local fermion number is imposed to project out the unphysical states and faithfully reproduce the physical Hilbert space. Substituting Eq. (2) into the J_1 - J_2 Hamiltonian Eq. (1), one obtains an interacting four-fermion system. Performing a mean-field decoupling would reformulate the interacting fermionic system to a quadratic level [14]. Specifically, by ignoring the pairing channel, the general quadratic spinon Hamiltonian with only spinon hopping sector is obtained as

$$H_{MF} = - \sum_{ij, \alpha} (t_{1,ij} f_{i,\alpha}^\dagger f_{j,\alpha} + t_{2,ij} f_{i,\alpha}^\dagger f_{j,\alpha} + h.c.) - \mu \sum_{i, \alpha} f_{i,\alpha}^\dagger f_{i,\alpha} \quad (3)$$

where we have maintained the SU(2) spin rotation symmetry of the original spin model and the local occupation constraint is relaxed such that only its average value satisfies $\sum_{\alpha} \langle f_{i\alpha}^\dagger f_{i\alpha} \rangle = 1$. The global chemical potential μ is introduced as a Lagrange multiplier to enforce such a constraint. Moreover, the mean-field parameters $t_{1,ij}$ and $t_{2,ij}$ represent the hopping amplitudes between NN and NNN sites, respectively. In the numerical studies, such as variational Monte Carlo approach, a similar mean-field Hamiltonian to Eq. (3) can also be exploited as a good starting point to construct the many-body variational wavefunction.

Here we stress again our purpose in the following is not to solve for the detailed ground state of a spin Hamiltonian as in Eq. (1). Instead, we assume that the system stabilizes a magnetically disordered QSL phase in the intermediate region $0.4 \lesssim J_2/J_1 \lesssim 0.6$, as suggested by a variety of numerical studies [21–25]. Comparing with pursuing solving a spin model exactly, it might be a better, or at least as a supplementary strategy to start from the potential QSL states and then single out the nontrivial and robust experimental signatures that allow us to distinguish a QSL. We then start from a mean-field theory to proceed with our analysis since much can already be learned from a mean-field investigation. A full treatment of the original spin model requires the involvement of all quantum fluctuations of the parameters around the mean-field solution, but the robust and intrinsic experimental signatures could maintain even the fluctuations are included.

The spinons fulfill the projective symmetries of the square lattice, and the mean-field parameters $t_{1,ij}$ and $t_{2,ij}$, also called mean-field ansatz in the literatures, should be constrained by a systematic projective symmetry group (PSG) analysis [14], which results in a classification of all possible QSLs. It is shown [14] that under open boundary condition of

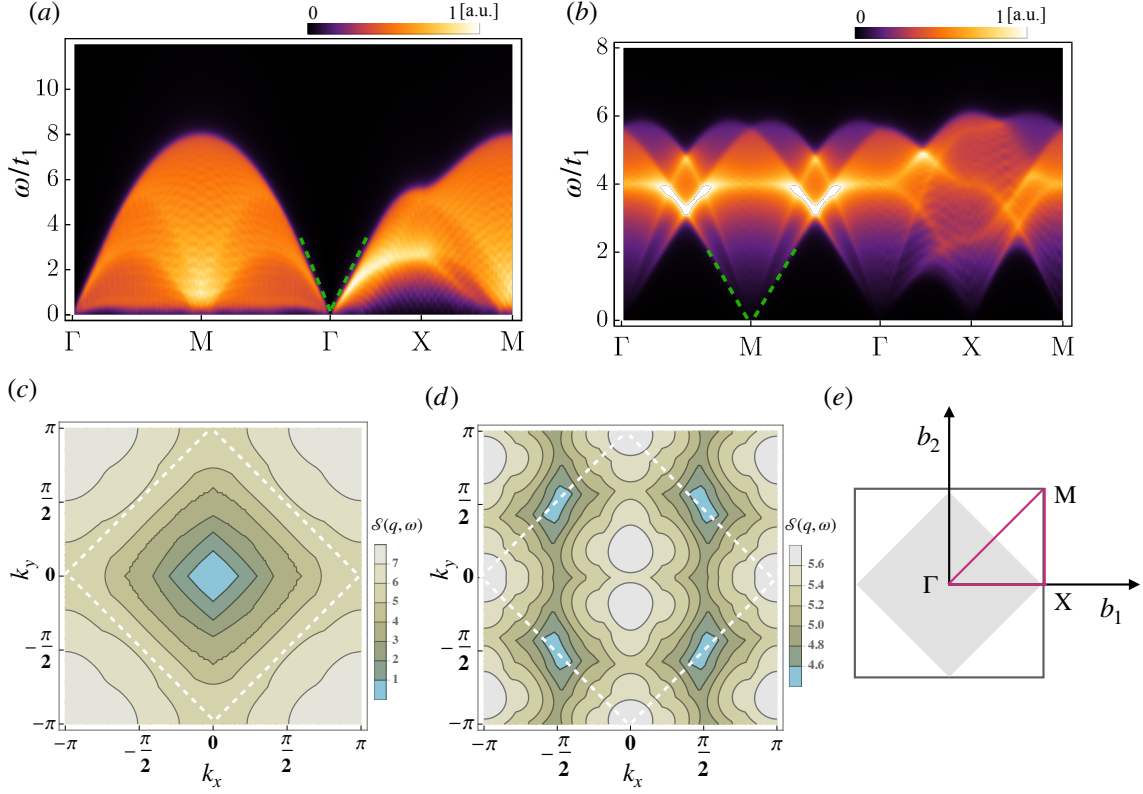


FIG. 2. (Color online.) Calculated dynamical spin structure factor $S(\mathbf{q}, \omega)$ along the high symmetry line Γ -M- Γ -X-M in the first Brillouin zone, (a) zero-flux spinon Fermi surface QSL with “V”-shape character around the Γ and (b) π -flux Dirac QSL with clear low-energy cone features around the high symmetry points. Contour plot of the upper edge of $S(\mathbf{q}, \omega)$ in the first Brillouin zone for (c) Zero-flux spinon Fermi surface QSL and (d) π -flux Dirac QSL. (e) Original Brillouin zone (outer black square) and the folded Brillouin zone (light gray square) of square lattice. The parameters adopted in the calculation are $t_2/t_1 = 0.2$ with zero temperature $k_B T/t_1 = 0$.

the square lattice, one can always fix the gauge such that the gauge transformations for translations satisfy

$$\mathcal{G}_{T_1}(i) = 1, \quad \mathcal{G}_{T_2}(i) = \eta_{xy}^{i_x + i_y}, \quad (4)$$

where T_1, T_2 are two translations of square lattice, and $\mathcal{G}_T(i)$ is the associated gauge transformation. The spinons thus fulfill the gauge enriched [14] translations $\tilde{T}_1 = \mathcal{G}_{T_1} T_1$ and $\tilde{T}_2 = \mathcal{G}_{T_2} T_2$. The parameter η_{xy} takes values ± 1 , then it divides all the possible QSLs on the lattice into two categories, i.e., zero-flux states correspond to $\eta_{xy} = +1$ and π -flux states correspond to $\eta_{xy} = -1$. In particular, the π -flux states harbor a fractionalized translation symmetry, which would result in a sharp signature in experiment. To illustrate this idea, we adopt the simplest two cases and the values of t_{ij} in Eq. (3) we have taken are shown in Fig. 1, where Fig. 1 (a) corresponds to a zero-flux QSL, while Fig. 1 (b) corresponds to a π -flux QSL. It can be easily verified that $t_{1,ij} = t_{1,ji} = -t_1$ on the (thick) red bonds in Fig. 1 (b) involve a background π gauge flux through the lattice, while this flux has no influence to the NNN hoppings. In fact, Figs. 1 (a) and (b) correspond to a spinon Fermi surface QSL and a π -flux Dirac QSL, respectively.

B. Inelastic neutron scattering spectrum and enhanced spectral periodicity

Inelastic neutron scattering (INS) measurement represents the best experimental probe to *directly* detect the magnetic excitations, and the dynamical information of excitations is encoded into the dynamical spin structure factor

$$\begin{aligned} \mathcal{S}(\mathbf{q}, \omega) &= \frac{1}{N} \sum_{i,j} e^{i\mathbf{q} \cdot (\mathbf{r}_i - \mathbf{r}_j)} \int dt e^{-i\omega t} \langle \mathbf{S}_i^-(t) \cdot \mathbf{S}_j^+(0) \rangle \\ &= \sum_n \delta[\omega - \xi_n(\mathbf{q})] |\langle n | \mathbf{S}_\mathbf{q}^+ | G \rangle|^2, \end{aligned} \quad (5)$$

where N is total number of lattice sites and the summation runs over all the excited eigenstates $|n\rangle$ with $\xi_n(\mathbf{q})$ being the energy of the n -th excited state with the momentum \mathbf{q} , while $|G\rangle$ stands for the spinon ground state with spinons filling the Fermi sea. In the numerical calculations, the delta function is taken to have a Lorentz broadening, $\delta(\omega) = \eta/[\pi(\omega^2 + \eta^2)]$ with $\eta = 0.1t_1$. Moreover, since $\mathbf{S}_\mathbf{q}^+ = \sum_{\mathbf{k}} f_{\mathbf{k}+\mathbf{q},\uparrow}^\dagger f_{\mathbf{k},\downarrow}$, the summation in Eq. (5) should be over all possible spin-1 excited states that are characterized by one spinon particle-hole pair crossing the spinon Fermi energy with a total energy

ω and total momentum \mathbf{q} [8]. In other words, the momentum-transfer \mathbf{q} and energy-transfer $\omega(\mathbf{q})$ of the neutron should be shared between the spinon particle-hole pair

$$\mathbf{q} = \mathbf{k}_1 - \mathbf{k}_2, \quad (6)$$

$$\xi(\mathbf{q}) = \omega_1(\mathbf{k}_1) - \omega_2(\mathbf{k}_2), \quad (7)$$

where $\omega_1(\mathbf{k})$ [$\omega_2(\mathbf{k})$] is the spinon (hole) excitation energy with momentum \mathbf{k} and the minus sign comes from the nature of hole excitation. The above equations indicate the two-spinon spectrum continuum, which is often count as a manifestation of fractionalized excitations, is a general character of QSLs. In Fig. 2 (a) and (b), we present the density plots of dynamical structure factor $\mathcal{S}(\mathbf{q}, \omega)$ along the high symmetry line Γ -M- Γ -X-M marked in Fig. 2 (e) for zero-flux QSL and π -flux QSL, respectively. As depicted in Fig. 2 (a), besides the obvious spectral continuum, a clear V-shape appears around Γ point, which originates from the particle-hole pair excitations crossing near the Fermi surface [8]. While for the π -flux Dirac QSL in Fig. 2 (b), the obvious phenomenon becomes the low-energy cone features that originate from the inter- (large \mathbf{q}) and intra-Dirac (small \mathbf{q}) cone scatterings, which is just the reflection of a Dirac QSL with Dirac band touching, *not* the π -flux for the spinons of the QSL. However, these signatures and evidences seem not to be strong enough to confirm a QSL, as it has been shown that a simple spectrum continuum, including the V-shape feature, in the dynamical spin structure factor can also be explained in the scenarios of usual glassy and disorder-induced states [11–13]. Therefore, additional signature of spectrum that is more unique to QSLs is expected to diagnose the fractionalized excitations.

For this purpose, next we consider the intrinsic fractionalized translation symmetry due to the π flux of the π -flux QSL. According to Eq. (4), the translation symmetries of spinons should satisfy

$$\tilde{T}_1 \tilde{T}_2 \tilde{T}_1^{-1} \tilde{T}_2^{-1} = \eta_{xy}, \quad (8)$$

where \tilde{T}_1 and \tilde{T}_2 are gauge enriched translations acting on the spinon degrees of freedom instead on the physical spins. For zero-flux state with $\eta_{xy} = 1$, the translations commute as usual, while for the π -flux state with $\eta_{xy} = -1$, the anti-commutation of translations implies a fractionalization of symmetry. It was first realized that the crystal momentum fractionalization of spinons has dramatic effects on the neutron spectrum [15, 16]. As a consequence, the periodicity of the upper excitation edge of the dynamic spin structure factor defined by

$$\text{edge}(\mathbf{q}) = \max_{\mathbf{k}} [\omega_1(\mathbf{k} + \mathbf{q}) - \omega_2(\mathbf{k})] \quad (9)$$

is doubled [27]. Therefore, for the zero-flux state, the upper two-spinon excitation edge should have the usual periodicity, while for the π -flux state, the upper two-spinon excitation edge exhibits an enhanced periodicity, that could serve as a sharp identification of fractionalized excitations beyond the simple spectrum continuum, since it is impossibly mimicked by any disorder-induced states. We illustrate the contour plots of the upper edge of the dynamic spin structure for the zero-flux QSL and π -flux QSL in Figs. 2 (c) and (d), respectively. It

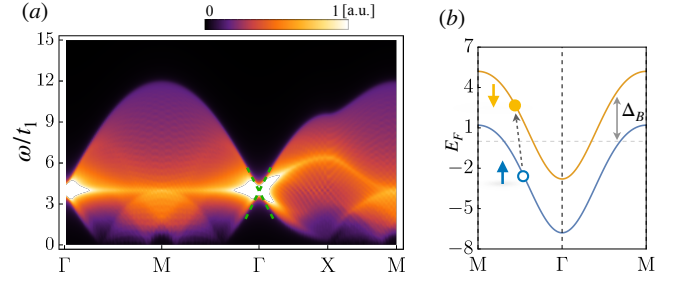


FIG. 3. (a) Dynamic spin structure factor for zero-flux QSL with $t_2/t_1 = 0.2$ and z -direction magnetic fields $B_z/t_1 = 4$. (b) Schematic illustration of the particle-hole excitations with small momenta. Such excitations for each \mathbf{q} are degenerate at zero field, while the two-fold degeneracy is lifted soon when the Zeeman field is turned on.

is clear that the π -flux QSL exhibits a fractionalization pattern with an enhanced periodicity in Fig. 2 (d), which is readily accessible to the INS measurements. The enhanced spectral periodicity with a folded Brillouin zone is the dynamical property rather than the static property and can not be captured by the static spin structure factor.

III. SPECTRUM CROSSING UNDER MAGNETIC FIELDS

In Sec. II, we have explicitly demonstrated that the excitation spectrum of the π -flux QSL would show an enhanced spectral periodicity in the reciprocal space, which is an intrinsic character of this kind of state and would be a strong evidence for QSL. Then a natural question is that for the zero-flux state, do we have any key features besides the simple spectral continuum to distinguish it from the glassy or disorder-induced states? In this section, we consider the field-driven behavior of a QSL. Under a moderate external magnetic field, the QSL phase should not be destroyed immediately, then we can safely consider the QSL behavior with fields. The fermionic spinon, unlike the usual electron, is electrical charge neutral and does not directly couple to the external magnetic field through the conventional orbital coupling. Especially in the strong Mott insulating regime that we focus in this section, there is only [28] a simple linear Zeeman coupling

$$H_B = -\frac{B_z}{2} \sum_{i,\alpha\beta} f_{i,\alpha}^\dagger \sigma_{\alpha\beta}^z f_{i,\beta}, \quad (10)$$

where we have considered the z -direction field for concreteness, and the Landé g factor and Bohr magneton μ_B have been absorbed in B_z . When the Zeeman term Eq. (10) enters the spinon Hamiltonian Eq. (3), a direct consequence would be the splitting spinon bands for spin- \uparrow and spin- \downarrow spinons, as show in Fig. 3 (b). At the zero momentum transfer, there should be a large density of spinon particle-hole excitations with the energy $\omega(\mathbf{q} = 0) = B_z$ due to the splitting bands.

To further observe how these splitting spinon bands reflect in the INS spectrum, we utilize the full zero-flux spinon

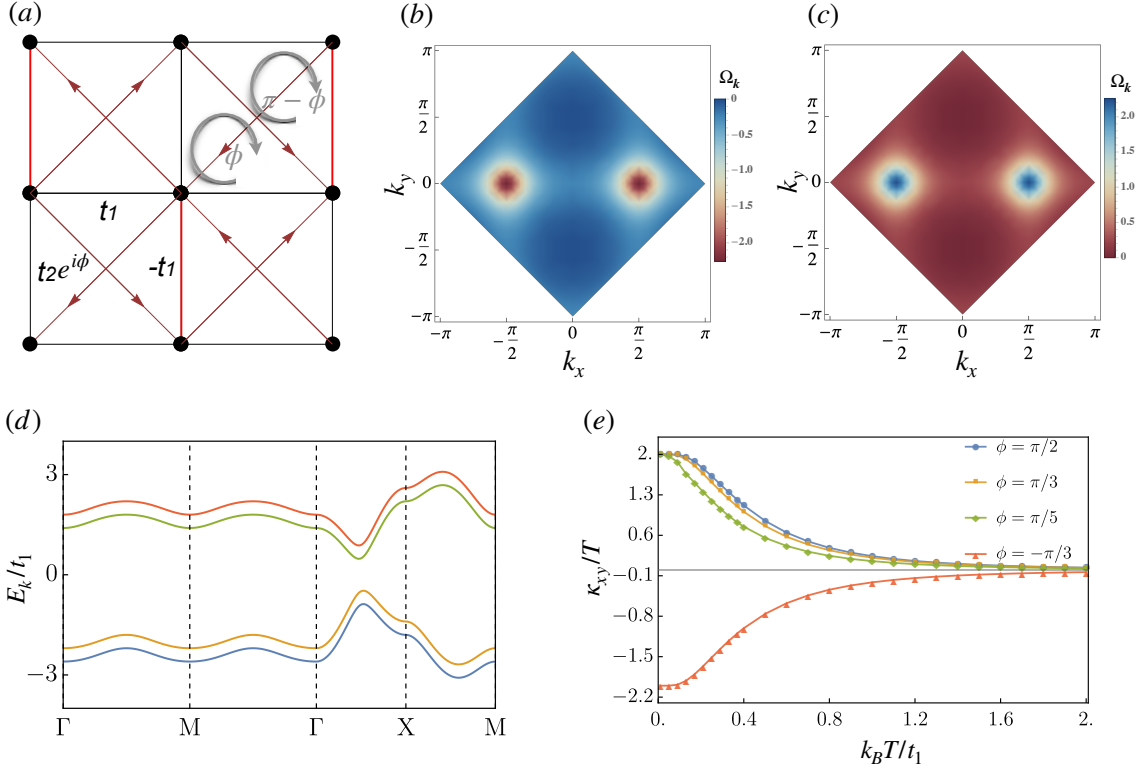


FIG. 4. (a) Schematic illustration of the spinon hopping matrix involving the complex second neighbor hopping coefficients, hopping along the arrows corresponds to ϕ , while hopping oppositely the arrows corresponds to $-\phi$. Contour plot of Berry curvatures calculated when $t_2/t_1 = 0.3$ and $\phi = \pi/2$ for (b) the lower two bands and (c) the upper two bands. (d) Representative spinon bands calculated when $t_2/t_1 = 0.2$, $\phi = \pi/3$ and $B_z/t_1 = 0.4$, the corresponding Chern numbers from the lowest band to the highest one are $-1, -1, +1, +1$, respectively. (e) The evolution of thermal Hall conductivity with temperature for different phase ϕ , where the magnetic field is fixed at $B_z/t_1 = 0.4$, and the unit of κ_{xy}/T here is $\pi k_B^2/6\hbar$.

Hamiltonian with Zeeman term to calculate the dynamical spin structure factor, the result is depicted in Fig. 3 (a). We note that the spectrum preserves the spinon continuum and remains gapless as expected, while the spectral weight at the Γ point is strongly enhanced at the band splitting energy $\omega = B_z$, well compatible with the large density of spinon particle-hole excitations with the energy B_z at zero momentum transfer. Besides the enhancement of the spectral intensity at the Γ point and the Zeeman splitting energy, the most interesting phenomenon is that the V-shaped spectrum around Γ point under zero field is recast into a X-shaped spectral crossing near the Zeeman splitting energy, which is a rather unique field-driven behavior for spinons originating from splitting spinon bands [28]. Therefore, we conclude that the X-shaped spectral crossing under Zeeman fields is another strong evidence for the QSL with spinon Fermi surface, since it is hard to imagine that the spin glassy or disorder-induced freezing states could reproduce such a spectral crossing under the magnetic fields.

IV. QUANTIZED THERMAL HALL EFFECT

In the previous two sections, we mainly focused on the INS spectral properties of the square lattice QSLs and suggest two strong signatures for QSLs, either from the intrinsic characters of QSLs or from the external field-driven behaviors. This is partly motivated by the fact that the spectral continuum of spin excitations detected by INS measurement is a direct evidence and consequence for the fractionalization. In this section, we turn to the thermal transport properties that can unveil the nature of the low-energy itinerant excitations. In the QSL phase, the deconfined spinons carry energy and thus transport heat under the temperature gradient field, same as the electrons transport charge in an electrical field. At the mean-field level where the spinons are nearly free, the spinon term should dominate the thermal conductivity κ_{xx} if spinons exist at low energies, and a finite residual of κ_{xx}/T in the low-temperature limit is proposed as the evidence for spinon Fermi surface or gapless spinon excitations, since the phonon contribution should be small at low temperatures. However, one should note that the total thermal conductivity in a Mott insulator (especially the the strong spin-orbit coupled Mott insulator) usually is not a simple addition of the magnetic contribution and the phonon contribution [29], while the mutual scattering

between the magnetic excitations and the phonons could suppress the value of κ_{xx} observed in the transport experiments. To obtain the smoking-gun signatures of QSLs, here we only focused on the thermal Hall effect of spinons as phonons usually do not contribute to thermal Hall transport.

Thermal Hall effect in QSLs is a rather nontrivial phenomenon since the spinon does not directly couple to external fields through conventional Lorentz coupling as we mentioned in Sec III. In a former work [30], we have pointed out that for the non-centrosymmetric U(1) QSLs with Dzyaloshinskii-Moriya (DM) interaction, the synergism of a moderate external magnetic field and DM interaction could effectively generate an internal U(1) gauge flux for the spinons and twists the spinon motion, which would result in a spinon thermal Hall effect under the temperature gradient field. This mechanism also has its limitation, as for the square lattice QSLs and other centrosymmetric QSLs, the DM interaction is usually prohibited by lattice symmetry [31, 32]. An alternative way is to consider the square lattice QSL in the weak Mott insulating regime, in which the strong charge fluctuations can bring the ring exchange spin interaction, and induce a scalar spin chiral term under fields [33–35]

$$H_\chi = J_\chi \sum_{i,j,k \in \triangle} \sin \Phi \mathbf{S}_i \cdot \mathbf{S}_j \times \mathbf{S}_k, \quad (11)$$

where the triangle \triangle for sums is formed by three neighbor sites involving two NN bonds and one NNN bond as shown in Fig. 4 (a), and Φ is the magnetic flux through the triangular plaquette in a counter clockwise way. A finite value of this term explicitly breaks the time reversal symmetry and parity, while their combination is well preserved. Moreover, decoupling this term to the quadratic level would induce a complex second neighbor hopping coefficient $t'_2 e^{i\theta_{ij}}$, thus the total NNN hopping amplitude should be

$$\begin{aligned} t_2 + t'_2 e^{i\theta_{ij}} &= (t_2 + t'_2 \cos \theta_{ij}) + it'_2 \sin \theta_{ij} \\ &= \sqrt{t_2^2 + t_2'^2 + 2t_2 t'_2 \cos(\theta_{ij})} e^{i\phi_{ij}} \\ &= t_2^* e^{i\phi_{ij}} \end{aligned} \quad (12)$$

where t_2^* is renormalized as $t_2^* = \sqrt{t_2^2 + t_2'^2 + 2t_2 t'_2 \cos(\theta_{ij})}$, and ϕ_{ij} is defined by $\tan(\phi_{ij}) = t'_2 \sin \theta_{ij} / (t_2 + t'_2 \cos \theta_{ij})$, in our case they are both tuning parameters and we can also denote the total NNN hopping coefficient as $t_2 e^{i\phi_{ij}}$ for simplicity of notation. A convenient convention of these hopping amplitudes is shown in Fig. 4 (a), where we have chosen the induced complex NNN hopping amplitudes on top of a π -flux QSL.

In this sense, the significance of external magnetic field B_z is *twofold*. It not only provides a linear Zeeman coupling to split the spinon bands, but also induces a complex NNN hopping coefficient that breaks the time reversal symmetry. Using the hopping matrix marked in Fig. 4 (a), we plot a typical spinon dispersion in Fig. 4 (d), where the fermion number constraint guarantees the bands to be half-filled, thus the lowest two spinon bands are fully occupied while the upper two spinon bands are completely empty, corresponding to

a gapped QSL state. According to Polyakov's argument for 2D compact U(1) gauge theory [36], if the state is trivially gapped, the dynamical U(1) gauge field will be confined due to the proliferation of monopoles and the system should enter a confining ordered state. However, the spinon Hamiltonian we considered is indeed nontrivial, since these spinon bands own non-vanishing Berry curvatures [see Figs. 4 (b) and (c) for the contour plots of the spinon Berry curvatures] and the total Chern number of the lowest two occupied bands is $C = -2 \neq 0$. Therefore, there would be a Chern-Simons term in the theory for gauge fluctuations and this state can safely get rid of the confinement issue, resulting in a CSL. Theoretically, the chiral edge modes of CSL would contribute to an integer quantized thermal Hall effect under temperature gradient field, which is the smoking-gun signature of a CSL.

To explicitly demonstrate the quantized thermal Hall effect and its evolution when varying temperature and the NNN hopping phase ϕ , we numerically calculate the thermal Hall conductivity for this QSL state. The thermal Hall conductivity formula is obtained [37] as

$$\kappa_{xy} = -\frac{k_B^2}{T} \int d\epsilon (\epsilon - \mu)^2 \frac{\partial f(\epsilon, \mu, T)}{\partial \epsilon} \sigma_{xy}(\epsilon), \quad (13)$$

where $f(\epsilon, \mu, T) = 1/[e^{\beta(\epsilon - \mu)} + 1]$ is the Fermi-Dirac distribution with chemical potential μ , and

$$\sigma_{xy}(\epsilon) = -\frac{1}{\hbar} \sum_{\mathbf{k}, \xi_{n,\mathbf{k}} < \epsilon} \Omega_{n,\mathbf{k}} \quad (14)$$

is the zero temperature Hall coefficient for a system with the chemical potential ϵ and Berry curvature $\Omega_{n\mathbf{k}} = -2\text{Im}\langle \partial u_{n\mathbf{k}} / \partial k_x | \partial u_{n\mathbf{k}} / \partial k_y \rangle$ for the spinon band indexed by n . Since in our case the chemical potential μ lies in the gap, in the zero temperature limit, Eq. (13) is recast into

$$\frac{\kappa_{xy}}{T} = -\frac{\pi k_B^2}{6\hbar} \sum_{n=1,2} C_n, \quad (15)$$

where C_n with $n = 1, 2$ is the Chern number of the two filled spinon bands. In Fig. 4 (e), we plot the evolution of κ_{xy}/T with temperature at various NNN hopping phase ϕ , the absolute value of them are all monotonically decreasing with increasing temperatures, and κ_{xy}/T gets smaller for smaller ϕ at the same nonzero temperature. In particular, the quantized number 2 in the zero temperature limit is consistent with theoretical analysis, and its sign depends on the sign of phase ϕ . If the CSL is induced by the external field through Eq. (11), the sign of phase ϕ should depend on the direction of field, thus the sign of thermal Hall conductivity also depends on the fields. In fact, a CSL may also be realized without applied fields and the quantized thermal Hall effect can be an intrinsic character. Overall, the quantized thermal Hall conductivity would be a particularly sharp signature for CSL. It is worth to note that the half-integer quantized thermal Hall effect has been reported [38] in the Kitaev QSL candidate α -RuCl₃ and is proposed to correspond to the chiral Majorana fermion edge mode.

V. DISCUSSION

In summary, we have highlighted three experimental schemes that would give smoking-gun signatures of QSLs including the thermal transport and spectrum measurements, and successfully applied them to square lattice QSLs. The π -flux QSL states would result in an enhanced spectral periodicity of the spinon continuum. It is the translation symmetry that is intrinsically fractionalized and renders such an enhanced spectral periodicity, much analogous to the fractional charge excitation in the fractional quantum Hall states where the global U(1) charge conservation gives the fractional charge quantum number to the fractionalized excitation. Under moderate magnetic fields when the description of QSL is still valid, the Zeeman coupling will enter the spinon Hamiltonian and lead to an X-shaped crossing of spectrum around Γ point, which is well compatible with the splitting bands for

spin- \uparrow , and spin- \downarrow spinons and is hard to be mimicked by the spin glass or disorder-induced states. Finally, if a CSL is realized, it would exhibit a quantized thermal Hall effect and a gapped spectrum. All of these sharp signatures can be robust even when the gauge fluctuations are included and do not depend on the geometry of underlying lattice, therefore we conclude these signatures could generally apply to other relevant QSLs.

ACKNOWLEDGMENTS

This work is supported by research funds from the Ministry of Science and Technology of China with grant No.2016YFA0301001, No.2018YFGH000095 and No.2016YFA0300500, from Shanghai Municipal Science and Technology Major Project with grant No.2019SHZDZX04, and from the Research Grants Council of Hong Kong with General Research Fund Grant No.17303819.

-
- [1] P. W. Anderson, *Science* **235**, 1196 (1987).
 - [2] A. Kitaev, *Annals of Physics* **321**, 2 (2006), january Special Issue.
 - [3] L. Balents, *Nature* **464**, 199 (2010).
 - [4] Y. Zhou, K. Kanoda, and T.-K. Ng, *Rev. Mod. Phys.* **89**, 025003 (2017).
 - [5] L. Savary and L. Balents, *Reports on Progress in Physics* **80**, 016502 (2016).
 - [6] P. Anderson, *Materials Research Bulletin* **8**, 153 (1973).
 - [7] T.-H. Han, J. S. Helton, S. Chu, D. G. Nocera, J. A. Rodriguez-Rivera, C. Broholm, and Y. S. Lee, *Nature* **492**, 406 (2012).
 - [8] Y. Shen, Y.-D. Li, H. Wo, Y. Li, S. Shen, B. Pan, Q. Wang, H. C. Walker, P. Steffens, M. Boehm, Y. Hao, D. L. Quintero-Castro, L. W. Harriger, M. D. Frontzek, L. Hao, S. Meng, Q. Zhang, G. Chen, and J. Zhao, *Nature* **540**, 559 (2016).
 - [9] C. Balz, B. Lake, J. Reuther, H. Luetkens, R. Schönmann, T. Herrmannsdörfer, Y. Singh, A. T. M. N. Islam, E. M. Wheeler, J. A. Rodriguez-Rivera, T. Guidi, G. G. Simeoni, C. Baines, and H. Ryll, *Nature Physics* **12**, 942 (2016).
 - [10] B. Gao, T. Chen, D. W. Tam, C.-L. Huang, K. Sasmal, D. T. Adroja, F. Ye, H. Cao, G. Sala, M. B. Stone, C. Baines, J. A. T. Verezhak, H. Hu, J.-H. Chung, X. Xu, S.-W. Cheong, M. Nallaiyan, S. Spagna, M. B. Maple, A. H. Nevidomskyy, E. Morosan, G. Chen, and P. Dai, *Nature Physics* **15**, 1052 (2019).
 - [11] Z. Ma, J. Wang, Z.-Y. Dong, J. Zhang, S. Li, S.-H. Zheng, Y. Yu, W. Wang, L. Che, K. Ran, S. Bao, Z. Cai, P. Čermák, A. Schneidewind, S. Yano, J. S. Gardner, X. Lu, S.-L. Yu, J.-M. Liu, S. Li, J.-X. Li, and J. Wen, *Phys. Rev. Lett.* **120**, 087201 (2018).
 - [12] I. Kimchi, A. Nahum, and T. Senthil, *Phys. Rev. X* **8**, 031028 (2018).
 - [13] Z. Zhu, P. A. Maksimov, S. R. White, and A. L. Chernyshev, *Phys. Rev. Lett.* **119**, 157201 (2017).
 - [14] X.-G. Wen, *Phys. Rev. B* **65**, 165113 (2002).
 - [15] A. M. Essin and M. Hermele, *Phys. Rev. B* **87**, 104406 (2013).
 - [16] A. M. Essin and M. Hermele, *Phys. Rev. B* **90**, 121102 (2014).
 - [17] G. Chen, *Phys. Rev. B* **96**, 085136 (2017).
 - [18] D. C. Tsui, H. L. Stormer, and A. C. Gossard, *Phys. Rev. Lett.* **48**, 1559 (1982).
 - [19] R. B. Laughlin, *Phys. Rev. Lett.* **50**, 1395 (1983).
 - [20] P. A. Lee, N. Nagaosa, and X.-G. Wen, *Rev. Mod. Phys.* **78**, 17 (2006).
 - [21] T. Li, F. Becca, W. Hu, and S. Sorella, *Phys. Rev. B* **86**, 075111 (2012).
 - [22] L. Capriotti, F. Becca, A. Parola, and S. Sorella, *Phys. Rev. Lett.* **87**, 097201 (2001).
 - [23] S.-L. Yu, W. Wang, Z.-Y. Dong, Z.-J. Yao, and J.-X. Li, *Phys. Rev. B* **98**, 134410 (2018).
 - [24] W.-J. Hu, F. Becca, A. Parola, and S. Sorella, *Phys. Rev. B* **88**, 060402 (2013).
 - [25] H.-C. Jiang, H. Yao, and L. Balents, *Phys. Rev. B* **86**, 024424 (2012).
 - [26] L. Sachdev, *Phys. Rev. B* **45**, 12377 (1992).
 - [27] Y.-D. Li, X. Yang, Y. Zhou, and G. Chen, *Phys. Rev. B* **99**, 205119 (2019).
 - [28] Y.-D. Li and G. Chen, *Phys. Rev. B* **96**, 075105 (2017).
 - [29] Y.-D. Li, Y.-M. Lu, and G. Chen, *Phys. Rev. B* **96**, 054445 (2017).
 - [30] Y. H. Gao and G. Chen, *SciPost Physics Core* **2**, 004 (2020).
 - [31] I. Dzyaloshinsky, *Journal of Physics and Chemistry of Solids* **4**, 241 (1958).
 - [32] T. Moriya, *Phys. Rev.* **120**, 91 (1960).
 - [33] D. Sen and R. Chitra, *Phys. Rev. B* **51**, 1922 (1995).
 - [34] O. I. Motrunich, *Phys. Rev. B* **73**, 155115 (2006).
 - [35] H. Katsura, N. Nagaosa, and P. A. Lee, *Phys. Rev. Lett.* **104**, 066403 (2010).
 - [36] A. Polyakov, *Nuclear Physics B* **120**, 429 (1977).
 - [37] T. Qin, Q. Niu, and J. Shi, *Phys. Rev. Lett.* **107**, 236601 (2011).
 - [38] Y. Kasahara, T. Ohnishi, Y. Mizukami, O. Tanaka, S. Ma, K. Sugii, N. Kurita, H. Tanaka, J. Nasu, Y. Motome, T. Shibauchi, and Y. Matsuda, *Nature* **559**, 227 (2018).